Static Friction between Silicon Nanowires and Elastomeric Substrates

Qingquan Qin and Yong Zhu*

Department of Mechanical & Aerospace Engineering, North Carolina State University, 911 Oval Drive, Campus Box 7910, Raleigh, North Carolina 27695, United States

ABSTRACT This paper reports the first direct measurements of static friction force and interfacial shear strength between silicon (Si) nanowires (NWs) and poly(dimethylsiloxane) (PDMS). A micromanipulator is used to manipulate and deform the NWs under a high-magnification optical microscope in real time. The static friction force is measured based on "the most-bent state" of the NWs. The static friction and interface shear strength are found to depend on the ultraviolet/ozone (UVO) treatment of PDMS. The shear strength starts at 0.30 MPa without UVO treatment, increases rapidly up to 10.57 MPa at 60 min of treatment and decreases for longer treatment. Water contact angle measurements suggest that the UVO-induced hydrophobic-to-hydrophilic conversion of PDMS surface is responsible for the increase in the static friction, while the hydrophobic recovery effect contributes to the decrease. The static friction between NWs and PDMS is of critical relevance to many device applications of NWs including NW-based flexible/stretchable electronics, NW assembly and nanocomposites (e.g., supercapacitors). Our results will enable quantitative interface design and control for such applications.

KEYWORDS: nanowire · PDMS · static friction · interfacial shear strength · adhesion · UVO treatment

One-dimensional (1D) nanomaterials have been used in a broad range of flexible/stretchable technologies ranging from photovoltaics and electronics to sensors and energy harvesting/storage.[1,2] In these flexible technologies, nanomaterials are typically bonded onto polymeric or plastic substrates. In addition to the competent electronic performance of these nanomaterials, their flexibility and interface interaction with the substrate also play important roles. Silicon (Si) nanowires (NWs) are one of the key building blocks for nanoscale electronic, photonic, and electromechanical devices.[3−5] For stretchable electronics, buckling-induced coiled or wavy shape of Si NWs on elastomeric substrates offers an effective approach to increase the stretchability of the devices.[6,7] In this case, the static friction (in the horizontal direction in contrast to the commonly used term, adhesion that is in the vertical direction) plays the key role in holding the NWs in deformed shapes.[6,7] In addition, scalable assembly of NWs is an enabling step for fabricating integrated, functional devices. The static friction between NWs and substrates is also critical in the NW assembly process.[8−10] Si NWs have been found to possess excellent mechanical properties including flexibility/stretchability.[11−13] However, the surface interaction between Si NWs and elastomeric substrates is largely unknown.

Atomic force microscope (AFM)-based single-asperity measurements have seen significant progress in nanoscale interface mechanics.[14−16] However, mechanics studies on the interfaces between 1D nanomaterials and substrates are limited.[17] For adhesion measurement, AFM or nanomanipulators were used to conduct peeling tests of nanostructures from a substrate or from each other;[18,19] for kinetic friction measurement, AFM or microfabricated devices were used to slide nanostructures on a substrate and record the friction force;[20,21] for static friction measurement, AFM or nanomanipulators were employed to manipulate/deform nanostructures either parallel or normal to a substrate.[17,22−26]

In this paper, we report direct measurements of the static friction force and interfacial shear strength between Si NWs and poly(dimethylsiloxane) (PDMS) for the first time. A micromanipulator was used to manipulate and deform the NWs under a high-magnification optical microscope. The static friction force was measured based on "the most-bent state" of the NWs.[22] The static friction and shear strength were found to increase rapidly and then decrease with the increasing ultraviolet/ozone (UVO) treatment of PDMS. Water contact angle on PDMS was independently measured as a function of the UVO treatment time, which suggested that the UVO-induced hydrophobic-to-hydrophilic conversion of the PDMS surface was responsible for the increase in static friction, while the hydrophobic recovery effect contributed to the decrease. PDMS possesses a unique combination of material properties including high stretchability over a wide temperature range, low toxicity, high electrical resistance, and long-term endurance, which makes it an important substrate material for flexible technologies.[1,27] The experimental

* Address correspondence to yong_zhu@ncsu.edu.

Received for review June 24, 2011 and accepted August 4, 2011.

Published online August 04, 2011
10.1021/nn202343w

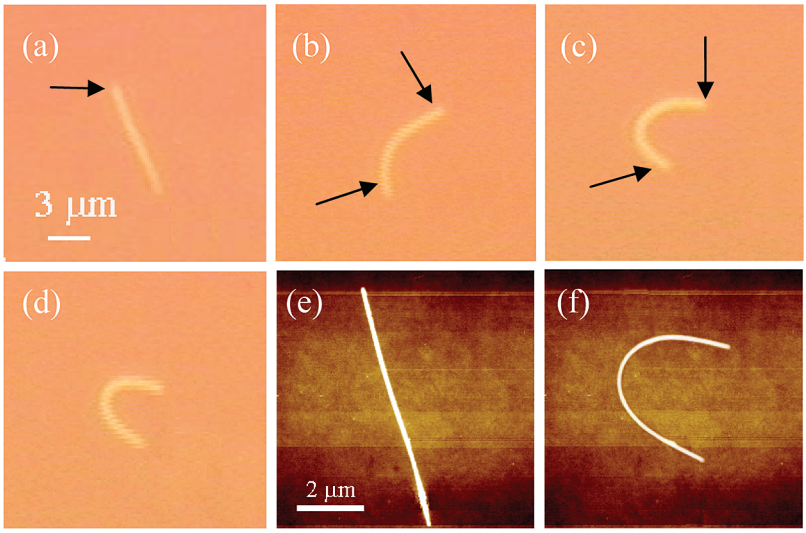

Figure 1. Optical and AFM images showing the manipulation process of a NW. (a−d) Optical images; (e,f) AFM images corresponding to (a) and (d), respectively.

method presented in this paper can be easily extended to other types of substrates (*e.g.*, plastics).

RESULTS AND DISCUSSION

A contact printing method was used to dry transfer the Si NWs[6,9] to the PDMS substrates. Subsequently, the friction measurements were carried out in a probe station (Micromanipulator 6200) under ambient condition (with temperature of the laboratory ~23 °C and the relative humidity ~50%). A tungsten probe was manually controlled to manipulate and deform NWs; the resolution of probe movement in all three orthogonal directions is 0.5 μm. The entire process was monitored under an optical microscope (1000× magnification). AFM (XE70, Park Systems) was used to take high-resolution images of the NWs before and after the manipulation. Figure 1 shows a typical NW manipulation process: (a−d) are optical images; (e) and (f) are AFM images corresponding to (a) and (d), respectively. The arrows indicate where the probe pushed the NW. The NW was progressively bent until a critical state was reached, which is the most-bent state. The shape of the NW results from competition between the elastic restoring force of the NW and the static friction at the NW/substrate interface.[22,23] At the critical state, the elastic restoring force is in equilibrium with the lateral static friction force along the NW. In order to ensure our NWs reached the most-bent state, we always bent them beyond this state (certainly without breaking them), as shown in Figure S1a in the Supporting Information. Upon retraction of the manipulator tip, the elastic restoring force was large enough to bring the NWs back to equilibrium, as shown in Figure S1b. The resolution of our micromanipulator (0.5 μm in this work) was not fine compared to AFM but sufficient for our purpose, indeed, because we always pushed a NW beyond the most-bent state and let the NW itself relax back. The advantage, however, was the real-time observation and easy control of the manipulation process.

In the following, we analyze the static friction force from the most-bent state.[24] This method assumes that bending deformation contributes predominantly to the strain energy, while the contributions due to axial stretching and transverse shear are negligible. In addition, this method assumes the NW slopes and curvatures are smooth (*i.e.*, no fracture or kinking), which is true for all the NWs in our experiments (as shown in Figure 2a). This is because Si NWs possess a large fracture strain as found in our previous work.[11]

In this method, the image of a bent NW was digitized using DataThief software[28] to obtain the Cartesian coordinates (x, y) of each centerline point along the NW. The curvature along the length of the NW is given by

$$\frac{d\theta}{ds}(s) = \frac{1}{\rho(s)} = \sqrt{\left[\frac{d^2x}{ds^2}(s)\right]^2 + \left[\frac{d^2y}{ds^2}(s)\right]^2} \quad (1)$$

where $\theta(s)$ is the angle between ds and dx, as indicated in Figure 2a, and $x(s)$ and $y(s)$ as function of s are shown in Figure S2. With the curvature along the NW known, the strain energy distribution per unit length, as shown in Figure 2b, is calculated

$$U_s(s) = \frac{EI}{2}\left[\frac{d\theta}{ds}(s)\right]^2 \quad (2)$$

where E is the elastic modulus and I is the moment of inertia of the NW ($I = (5\sqrt{3})/(144)D^4$, D is the diameter of the NW). Considering the size effect on elastic modulus of Si NWs, the size-dependent modulus is used in our analysis.[11] Note that Si NWs in this work are oriented in the [111] direction and possess hexagonal cross sections.[11,29] D is the height of the NW (distance between two parallel edges of the hexagon) as measured by AFM.

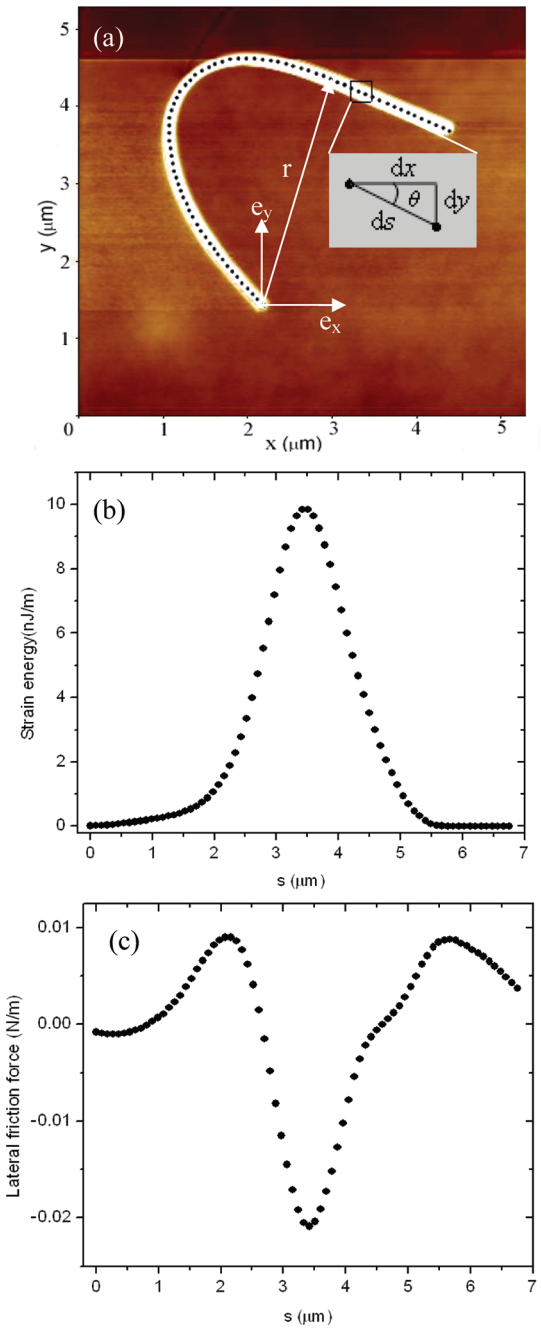

Figure 2. (a) AFM image of a NW at the most-bent state, where the data points were digitized using DataThief. The geometric relationship was shown in the inset. (b,c) Strain energy and lateral friction force distribution along the NW shown in (a), respectively.

The lateral friction force per unit length, as shown in Figure 2c, is related to the third derivative of $\theta(s)$

$$f(s) = -EI\frac{d^3\theta}{ds^3}(s) \qquad (3)$$

The static friction force per unit length (F) is the maximum lateral friction force along the length of the NW at the most-bent state. The interfacial shear strength (τ) is the static friction force per unit length divided by the contact width. A key step in this analysis

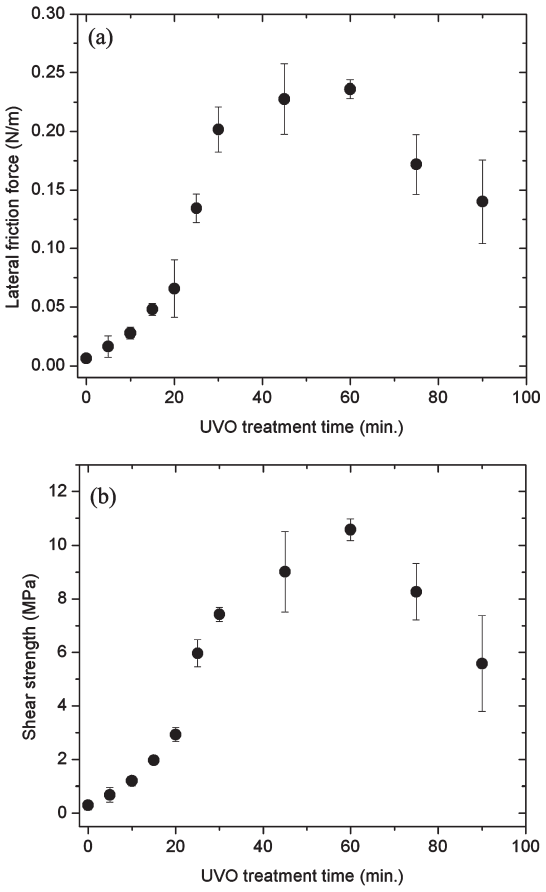

Figure 3. (a) Static friction force and (b) interfacial shear strength between Si NWs and PDMS substrate at different UVO treatment times.

method is the numerical differentiation (derivative) as involved in all three equations. The data are smoothed using a five-point moving average method before the numerical differentiation;[30] the first derivative data are also smoothed using the five-point moving average method before the second derivative; this process is repeated until the third derivative of $\theta(s)$ is obtained. We emphasize that this analysis method is theoretically accurate; the approximation comes from the numerical differentiation. Our smoothing-differentiation procedure turned out to yield reliable friction force data, as shown in Figure 3.

Figure 3a shows the static friction force per unit length between Si NWs and PDMS as a function of UVO treatment time. For each treatment time, three to five NWs were tested. All of the NWs used in this study ranged from 35 to 55 nm in diameter (D) and 4−8 μm in length. For treatment time less than 20 min, the friction force increased modestly from 0.006 to 0.06 N/m. When the treatment time increased from 20 to 45 min, a rapid increase in friction force was observed. The friction force decreased for longer treatment time (beyond 60 min). In addition, no dependence on the NW orientation on the substrate was found in all of our experiments.

To calculate shear strength between Si NWs and PDMS, one needs to determine the true contact area between them, which is nontrivial.[14] Since the NWs are long and compliant, they are expected to have intimate contact with the substrate,[20] especially considering the roughness of the PDMS substrate before or after the UVO treatment is very small (as shown in Figure S4). In addition, our measurement is local in nature; the static friction (*i.e.*, maximum lateral friction as measured following eq 3) is expected to occur at a specific location. Therefore, we assume the contact area is the flat side surface of the NW. The shear strength τ was obtained by setting the contact width $w = D/\sqrt{3}$ (for hexagonal cross sections as for the Si NWs used in our work). The maximum shear strength was *ca.* 10.57 MPa at 60 min of UVO treatment, as shown in Figure 3b.

PDMS is a silicon-based rubber material with highly hydrophobic surfaces. Various techniques have been utilized to modify the surface properties of PDMS.[31,32] As part of the oxygen plasma treatment family, UVO treatment converts the $-OSi(CH_3)_2-$ groups on PDMS surface into $-O_nSi(OH)_{4-n}$ terminated groups[27] and forms a thin and brittle silica-like layer on the surface. The increase of silanol groups (Si−OH) is at the expense of methyl groups ($-CH_3$); X-ray photoelectron spectroscopy (XPS) study of atomic composition of PDMS surface revealed that the carbon content decreased, the oxygen content increased, while the silicon content remained almost unchanged with increasing exposure time.[33−35] As silanol groups are polar in nature, UVO-treated PDMS surface becomes highly hydrophilic and can react with various inorganic surfaces such as glass, silicon, silicon oxide, and quartz to form strong siloxane (Si−O−Si) bonds through condensation reactions.[27] UVO treatment is very similar to the oxygen plasma treatment in the surface modification of PDMS, except that UVO treatment is a much milder process. UVO treatment of PDMS has been widely used in sealing microfluidic channels,[27] increasing adhesion force for soft lithography,[36] and fabricating stretchable electronic devices.[37]

Without UVO treatment, the interaction between Si NWs and PDMS was based on van der Waals force. The shear strength value measured in our experiments (0.30 MPa) is much smaller than those obtained with AFM measurements.[14,38] On the other hand, in several experiments with pushing nanoparticles or NWs on substrates, values as small as 0.05−1 MPa were indeed reported.[21,39,40] Moreover, our results are in close agreement with the static friction measurements between InAs NWs and silicon oxide or silicon nitride substrates.[22,23] With the UVO treatment, the interaction was based on chemical bonding (siloxane bond). The concentrations of the surface methyl groups and siloxane bonds decreased and increased, respectively, in an exponential fashion with the UVO treatment time.[41] This agreed very well

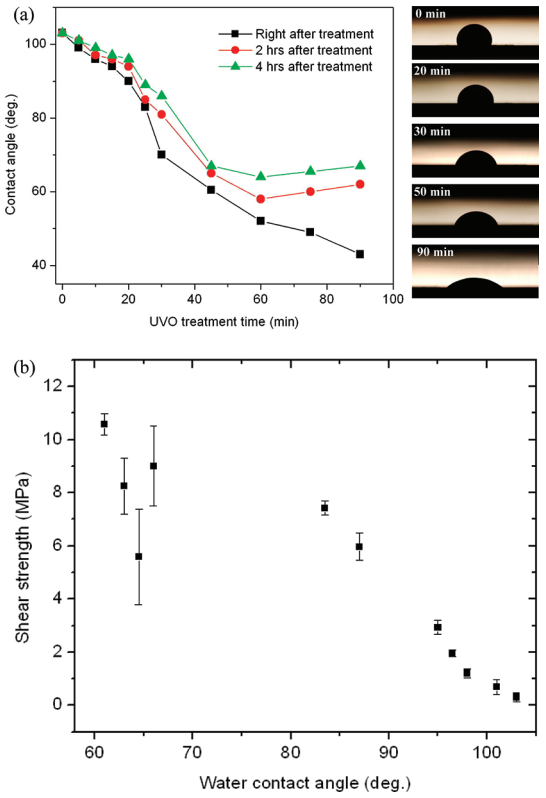

Figure 4. (a) (Left) water contact angle as a function of UVO treatment time and (right) images showing water contact angles at different treatment times (0, 20, 30, 50, and 90 min, immediately after UVO treatment). (b) Shear strength as a function of water contact angle. The water contact angle is the average value of those 2 and 4 h after UVO treatment. The increase of shear strength is in line with the decrease of water contact angle.

with the rapid increase in the shear strength for UVO treatment up to 30 min as observed in our case.

The effect of UVO treatment on PDMS was independently investigated by water contact angle measurements. The change of water contact angle is directly related to the concentration of surface hydrophilic functional groups.[42] Figure 4a shows water contact angle as a function of the UVO treatment time. For a given treatment time, the contact angle was measured three times, 0 (immediately), 2, and 4 h after the treatment, respectively; 2 and 4 h were chosen here since the manipulation process of NWs (for friction measurement) typically took 2−4 h. The water contact angle decreased with the increase of UVO treatment time. Decrease of the contact angle is indicative of increase of the hydrophilic groups on the surface[33,43,44] and thus increase of chances to form chemical bonds with Si NWs. The contact angle measurement was consistent with our friction force measurement. Figure 4b plots shear strength as a function of water contact angle (average value of the 2 and 4 h post-treatments). This confirmed that the increase of hydrophilic groups on the PDMS surface was responsible for the increase in static friction force and shear strength. The bond strength and water contact angle between

plasma-treated PDMS and glass showed similar relationship at relatively short treatment time.[45] We note that relative large scatter in the shear strength exists for the water contact angle between 60 and 70°. For this range of water contact angle, the UVO treatment time was quite long (45, 60, 75, and 90 min), and the hydrophobic recovery effect (to be discussed) was pronounced. The water contact angle highly depended on the post-treatment time especially for the long UVO treatment time (see Figure 4a). The NW manipulation process typically took 2−4 h. It is likely that the large scatter is due to the uncertainty in the post-treatment time when the NW manipulation was conducted.

It is interesting to note that the friction force and shear strength decreased for UVO treatment over 60 min. A similar behavior was observed previously in the bond strength between plasma-treated PDMS and glass;[45,46] it was attributed to the formation of cracks on the PDMS surface and the increase in surface roughness when overexposed. We characterized the UVO-treated PDMS surface with AFM and scanning electron microscopy (SEM); however, no crack was found for a treatment time up to 120 min, as shown in Supporting Information Figure S3. Noncontact AFM imaging of UVO-treated PDMS revealed that surface roughness (*Rq*) actually decreased for short treatment time and remained nearly constant for longer treatment time, as shown in Supporting Information Figure S4. For each treatment time, the roughness data were obtained from at least three different locations on the surface. Our results ruled out the contributions of cracks and increasing surface roughness to the observed decrease of friction force.

Surface hydrophobic recovery is likely the major mechanism for the decrease in friction force at longer treatment time. Free low-mass-molar chains, which are formed by chain scission reactions during the UVO treatment or intrinsically present as residues from the polymerization in PDMS preparation, could migrate to the surface after the treatment.[47] Excessive silanol bonds on the surface lead to surface chain scission reactions and reduce the number of silanol bonds.[45] As a result, the density of the siloxane bonds with Si NWs decreases and so does the static friction. Such an effect becomes more pronounced with the increasing post-treatment time. Surface hydrophobic recovery has been observed by the water contact angle measurement and XPS study.[33] Our water contact angle measurements also revealed such a recovery effect; see Figure 4a. The recovery effect was dependent on the post-treatment time in addition to the treatment time. The recovery effect was stronger for longer treatment time; for the same treatment time, the recovery effect increased with the increasing post-treatment time. For UVO treatment longer than 60 min, the recovery effect was so pronounced that the contact angle even started increasing after 2 h of post-treatment. The water contact angle measurements strongly suggested that surface hydrophobic recovery was responsible for the observed decrease of friction force.

CONCLUSIONS

We have reported direct measurements of static friction force and interfacial shear strength between Si NWs and PDMS substrate. UVO treatment was found to convert the unmodified hydrophobic surface of PDMS to a highly polar and reactive surface, which formed strong siloxane bonds with Si NWs. As a result, the static friction force increased to the maximum value of ~0.236 N/m at ~60 min of UVO treatment, corresponding to the shear strength of 10.57 MPa. The effect of hydrophobic recovery of the treated PDMS surface contributed to the decrease in friction force at longer treatment time. The static friction between NWs and PDMS plays a critical role to hold the NWs in deformed shapes, which is important for a variety of applications ranging from NW assembly to NW-based flexible electronics and sensors to nanocomposites (e.g., supercapacitors).[48] Our measurements will contribute to rational interface design and control for such applications. Furthermore, quantifying the effect of UVO treatment on PDMS provides valuable guidelines for selectively tuning the interactions at NW/PDMS interfaces, which might provide a simple route for patterned printing of NWs on PDMS.[2,49] The methodology presented in this study can be used to investigate static friction between other types of 1D nanomaterials (*e.g.*, carbon nanotubes) and substrates (*e.g.*, plastics).

METHODS

Preparation of Si NWs and PDMS. Si NWs were synthesized on Si substrates by chemical vapor deposition (CVD) using gold nanoclusters as catalysts and silane (SiH_4) as a vapor-phase reactant, following the method reported previously.[3,29] PDMS substrates with a thickness of 2 mm were prepared using Sylgard 184 (Dow Corning) by mixing the base and the curing agent with a ratio of 10:1. The mixture was first placed in a vacuum oven to remove air bubbles and then cured at 65 °C for 12 h. Rectangular slabs of suitable sizes were cut from the cured piece.

NW Manipulation Process. NW manipulation was performed in ambient condition on a probe station. A tungsten probe (7B-2 from Micromanipulator Company Inc.) was mounted to the micromanipulator, which can move in three directions. Every NW was bent beyond the most-bent state and then relaxed to the most-bent state after retracting the manipulator probe (Figure S1). The competition between lateral friction force and elastic restoring force brings the NW back to an equilibrium state. Most NWs used in this study ranged from ~4 to ~8 μm in length.

UVO Treatment of PDMS. The PDMS slabs were radiated under the UV lamp (low-pressure mercury lamp, 30 μW/cm^2 for

254 nm and 16 μW/cm^2 for 185 nm at the distance of 20 cm from the lamp, BHK) with the assistance of UV-generated ozone. UVO treatment is a photosensitized oxidation process in which the molecules of the treated material are excited and/or dissociated by the absorption of short-wavelength UV radiation. The UV-light-induced ozone converts the unmodified hydrophobic surface of PDMS dominated by $-Si(CH_3)_2O-$ groups to a highly polar and reactive surface terminated with silanol groups ($-SiOH$). In addition, the UVO treatment generates a silica-like layer (SiO_x containing a small amount of carbon) on the surface of PDMS.[41,43,50]

Contact Angle Measurement. The water contact angle was measured using the sessile drop method. The experiments were performed using a simple custom-made setup that includes a CCD camera, a horizontal stand, a light source, a syringe, and syringe holder. PDMS samples were placed on the horizontal stand. The syringe was fixed vertically about 4 mm on top of the PDMS surface using the syringe holder. Static contact angle was measured by applying a single drop of deionized (DI) water to the PDMS surface. Each data point reported in this paper represents an average of five measurements on different areas of the same sample and has an error less than $\pm 2.5°$.

Acknowledgment. This work was supported by the National Science Foundation under Award Nos. CMMI-0826341 and 1030637. We sincerely thank Professor Wei Lu for providing the Si NWs used in this study, and Professor Tiegang Fang for help with the contact angle measurement.

Supporting Information Available: (1) Images showing "the most-bent state" in manipulation process. (2) Figure showing digitalized data *x* and *y* as a function of *s*. (3) SEM images of PDMS surface before and after UVO treatment. (4) AFM measurement of the PDMS surface roughness. This material is available free of charge *via* the Internet at http://pubs.acs.org.

REFERENCES AND NOTES

1. Rogers, J. A.; Someya, T.; Huang, Y. Materials and Mechanics for Stretchable Electronics. *Science* **2010**, *327*, 1603–1607.
2. Fan, Z.; Ho, J. C.; Takahashi, T.; Yerushalmi, R.; Takei, K.; Ford, A. C.; Chueh, Y.-L.; Javey, A. Toward the Development of Printable Nanowire Electronics and Sensors. *Adv. Mater.* **2009**, *21*, 3730–3743.
3. Lu, W.; Lieber, C. M. Semiconductor Nanowires. *J. Phys. D: Appl. Phys.* **2006**, *39*, R387–R406.
4. Duan, X.; Niu, C.; Sahi, V.; Chen, J.; Parce, J. W.; Empedocles, S.; Goldman, J. L. High-Performance Thin-Film Transistors Using Semiconductor Nanowires and Nanoribbons. *Nature* **2003**, *425*, 274–278.
5. McAlpine, M. C.; Ahmad, H.; Wang, D.; Heath, J. R. Highly Ordered Nanowire Arrays on Plastic Substrates for Ultrasensitive Flexible Chemical Sensors. *Nat. Mater.* **2007**, *6*, 379–384.
6. Xu, F.; Lu, W.; Zhu, Y. Controlled 3D Buckling of Silicon Nanowires for Stretchable Electronics. *ACS Nano* **2011**, *5*, 672–678.
7. Ryu, S. Y.; Xiao, J. L., II; Park, W.; Son, K. S.; Huang, Y. Y.; Paik, U.; Rogers, J. A. Lateral Buckling Mechanics in Silicon Nanowires on Elastomeric Substrates. *Nano Lett.* **2009**, *9*, 3214–3219.
8. Fan, Z. Y.; Ho, J. C.; Jacobson, Z. A.; Yerushalmi, R.; Alley, R. L.; Razavi, H.; Javey, A. Wafer-Scale Assembly of Highly Ordered Semiconductor Nanowire Arrays by Contact Printing. *Nano Lett.* **2008**, *8*, 20–25.
9. Xu, F.; Durham, J. W.; Wiley, B. J.; Zhu, Y. Strain-Release Assembly of Nanowires on Stretchable Substrates. *ACS Nano* **2011**, *5*, 1556–1563.
10. Javey, A.; Nam, S.; Friedman, R. S.; Yan, H.; Lieber, C. M. Layer-by-Layer Assembly of Nanowires for Three-Dimensional, Multifuctional Electronics. *Nano Lett.* **2007**, *7*, 773–777.
11. Zhu, Y.; Xu, F.; Qin, Q.; Fung, W. Y.; Lu, W. Mechanical Properties of Vapor–Liquid–Solid Synthesized Silicon Nanowires. *Nano Lett.* **2009**, *9*, 3934–3939.
12. Hoffmann, S.; Utke, I.; Moser, B.; Michler, J.; Christiansen, S. H.; Schmidt, V.; Senz, S.; Werner, P.; Gosele, U.; Ballif, C. Measurement of the Bending Strength of Vapor–Liquid–Solid Grown Silicon Nanowires. *Nano Lett.* **2006**, *6*, 622–625.
13. Li, X. D.; Bhushan, B. Fatigue Studies of Nanoscale Structures for MEMS/NEMS Applications Using Nanoindentation Techniques. *Surf. Coat. Technol.* **2003**, *163*, 521–526.
14. Carpick, R. W.; Salmeron, M. Scratching the Surface: Fundamental Investigations of Tribology with Atomic Force Microscopy. *Chem. Rev.* **1997**, *97*, 1163–1194.
15. Szlufarska, I.; Chandross, M.; Carpick, R. W. Recent Advances in Single-Asperity Nanotribology. *J. Phys. D: Appl. Phys.* **2008**, *41*, 123001.
16. Bhaskaran, H.; Gotsmann, B.; Sebastian, A.; Drechsler, U.; Lantz, M. A.; Despont, M.; Jaroenapibal, P.; Carpick, R. W.; Chen, Y.; Sridharan, K. Ultralow Nanoscale Wear through Atom-by-Atom Attrition in Silicon-Containing Diamond-like Carbon. *Nat. Nanotechnol.* **2010**, *5*, 181–185.
17. Falvo, M. R.; Superfine, R. Mechanics and Friction at the Nanometer Scale. *J. Nanopart. Res.* **2000**, *2*, 237–248.
18. Strus, M. C.; Zalamea, L.; Raman, A.; Pipes, R. B.; Nguyen, C. V.; Stach, E. A. Peeling Force Spectroscopy: Exposing the Adhesive Nanomechanics of One-Dimensional Nanostructures. *Nano Lett.* **2008**, *8*, 544–550.
19. Ke, C.; Zheng, M.; Zhou, G.; Cui, W.; Pugno, N.; Miles, R. N. Mechanical Peeling of Free-Standing Single-Walled Carbon-Nanotube Bundles. *Small* **2010**, *6*, 438–445.
20. Manoharan, M. P.; Haque, M. A. Role of Adhesion in Shear Strength of Nanowire–Substrate Interfaces. *J. Phys. D: Appl. Phys.* **2009**, *42*, 095304.
21. Sheehan, P. E.; Lieber, C. M. Nanotribology and Nanofabrication of MoO_3 Structures by Atomic Force Microscopy. *Science* **1996**, *272*, 1158–1161.
22. Bordag, M.; Ribayrol, A.; Conache, G.; Froberg, L. E.; Gray, S.; Samuelson, L.; Montelius, L.; Petterson, H. Shear Stress Measurements on InAs Nanowires by AFM Manipulation. *Small* **2007**, *3*, 1398–1401.
23. Conache, G.; Gray, S. M.; Ribayrol, A.; Froberg, L. E.; Samuelson, L.; Petterson, H.; Montelius, L. Friction Measurements of InAs Nanowires on Silicon Nitride by AFM Manipulation. *Small* **2009**, *5*, 203–207.
24. Strus, M. C.; Lahiji, R. R.; Ares, P.; Lopez, V.; Raman, A.; Reifenberger, R. Strain Energy and Lateral Friction Force Distributions of Carbon Nanotubes Manipulated into Shapes by Atomic Force Microscopy. *Nanotechnology* **2009**, *20*, 385709.
25. Zhu, Y.; Qin, Q.; Gu, Y.; Wang, Z. Friction and Shear Strength at the Nanowire–Substrate Interfaces. *Nanoscale Res. Lett.* **2010**, *5*, 291–295.
26. Falvo, M. R.; Clary, G. J.; Taylor, R. M.; Chi, V.; Brooks, F. P.; Washbum, S.; Superfine, R. Bending and Buckling of Carbon Nanotubes under Large Strain. *Nature* **1997**, *389*, 582–584.
27. Duffy, D. C.; McDonald, J. C.; Schueller, O. J. A.; Whitesides, G. M. Rapid Prototyping of Microfluidic Systems in Poly(dimethylsiloxane). *Anal. Chem.* **1998**, *70*, 4974–4984.
28. Tummers, B. *DataThief III* 2006, http://datathief.org.
29. Wu, Y.; Cui, Y.; Huynh, L.; Barrelet, C. J.; Bell, D. C.; Lieber, C. M. Controlled Growth and Structures of Molecular-Scale Silicon Nanowires. *Nano Lett.* **2004**, *4*, 433–436.
30. Zhu, Y.; Liechti, K. M.; Ravi-Chandar, K. Direct Extraction of Rate-Dependent Traction-Separation Laws for Polyurea/Steel Interfaces. *Int. J. Solids Struct.* **2009**, *46*, 31–51.
31. Thanawala, S. K.; Chaudhury, M. K. Surface Modification of Silicone Elastomer Using Perfluorinated Ether. *Langmuir* **2000**, *16*, 1256–1260.
32. Chaudhury, M. K. SurfaceFree Energies of Alkylsiloxane Monolayers Supported on Elastomeric Polydimethylsiloxanes. *J. Adhes. Sci. Technol.* **1993**, *7*, 669–675.
33. Olah, A.; Hillborg, H.; Vancso, G. J. Hydrophobic Recovery of UV/Ozone Treated Poly(dimethylsiloxane): Adhesion Studies by Contact Mechanics and Mechanism of Surface Modification. *Appl. Surf. Sci.* **2005**, *239*, 410–423.

34. Egitto, F. D.; Matienzo, L. J. Transformation of Poly(dimethylsiloxane) into Thin Surface Films of SiO_x by UV/Ozone Treatment. Part I: Factors Affecting Modification. *J. Mater. Sci.* **2006**, *41*, 6362–6373.
35. Graubner, V.-M.; Jordan, R.; Nuyken, O.; Schnyder, B.; Lippert, T.; Kotz, R.; Wokaum, A. Photochemical Modification of Cross-Linked Poly(dimethylsiloxane) by Irradiation at 172 nm. *Macromolecules* **2004**, *37*, 5936–5943.
36. Thangawng, A. L.; Swartz, M. A.; Glucksberg, M. R.; Ruoff, R. S. Bond−Detach Lithography: A Method for Micro/Nanolithography by Precision PDMS Patterning. *Small* **2007**, *3*, 132–138.
37. Kim, D.; Xiao, J.; Huang, Y.; Rogers, J. A. Stretchable, Curvilinear Electronics Based on Inorganic Materials. *Adv. Mater.* **2010**, *22*, 2108–2124.
38. Xu, D.; Ravi-Chandar, K.; Liechti, K. M. On Scale Dependence in Friction: Transition From Intimate to Monolayer-Lubricated Contact. *J. Colloid Interface Sci.* **2008**, *318*, 507–519.
39. Meyer, M.; Overney, R.; Brodbeck, D.; Howald, L.; Luthi, R.; Frommer, J.; Guntherodt, H.-J. Friction and Wear of Langmuir−Blodgett Films Observed by Friction Force Microscopy. *Phys. Rev. Lett.* **1992**, *69*, 1777–1780.
40. Luthi, R.; Meyer, E.; Haefke, H.; Howald, L.; Gutmannsbauer, W.; Guntherodt, H.-J. Sled-Type Motion on the Nanometer Scale: Determination of Dissipation and Cohesive Energies of C_{60}. *Science* **1994**, *266*, 1979–1981.
41. Ye, H.; Gu, Z.; Gracias, D. H. Kinetics of Ultraviolet and Plasma Surface Modification of Poly(dimethylsiloxane) Probed by Sum Frequency Vibrational Spectroscopy. *Langmuir* **2006**, *22*, 1863–1868.
42. Rinsch, C. L.; Chen, X.; Panchalingam, V.; Eberhart, R. C.; Wang, J.; Timmons, R. B. Pulsed Radio Frequency Plasma Polymerization of Allyl Alcohol: Controlled Deposition of Surface Hydroxyl Groups. *Langmuir* **1996**, *12*, 2995–3002.
43. Fu, Y.-J.; Qui, H.-z.; Liao, K.-S.; Lue, S. J.; Hu, C.-C.; Lee, K.-R.; Lai, J.-Y. Effect of UV-Ozone Treatment on Poly(dimethylsiloxane) Membranes: Surface Characterization and Gas Separation Performance. *Langmuir* **2010**, *26*, 4392–4399.
44. Efimenko, K.; Wallace, W. E.; Genzer, J. Surface Modification of Sylgard-184 Poly(dimethyl siloxane) Networks by Ultraviolet and Ultraviolet/Ozone Treatment. *J. Colloid Interface Sci.* **2002**, *254*, 306–315.
45. Bhattacharya, S.; Datta, A.; Berg, J. M.; Gangopadhyay, S. Studies on Surface Wettability of Poly(dimethyl) Siloxane (PDMS) and Glass under Oxygen-Plasma Treatment and Correlation with Bond Strength. *J. Microelectromech. Syst.* **2005**, *14*, 590–597.
46. Millare, B.; Thomas, M.; Ferreira, A.; Xu, H.; Holesinger, M.; Vullev, V. I. Dependence of the Quality of Adhesion between Poly(dimethylsiloxane) and Glass Surfaces on the Conditions of Treatment with Oxygen Plasma. *Langmuir* **2008**, *24*, 13218–13224.
47. Kim, J.; Chaudhury, K.; Owen, M. J. Hydrophobic Recovery of Polydimethylsiloxane Elastomer Exposed to Partial Electrical Discharge. *J. Colloid Interface Sci.* **2000**, *226*, 231–236.
48. Bao, L.; Zang, J.; Li, X. D. Flexible Zn_2SnO_4/MnO_2 Core/Shell Nanocable−Carbon Microfiber Hybrid Composites for High-Performance Supercapacitor Electrodes. *Nano Lett.* **2011**, *11*, 1215–1220.
49. Takahashi, T.; Takei, K.; Ho, J. C.; Chueh, Y.-L.; Fan, Z.; Javey, A. Monolayer Resist for Patterned Contact Printing of Aligned Nanowire Arrays. *J. Am. Chem. Soc.* **2009**, *131*, 2102–2103.
50. Ouyang, M.; Yuan, C.; Muisener, R. J.; Boulares, A.; Koberstein, J. T. Conversion of Some Siloxane Polymers to Silicon Oxide by UV/Ozone Photochemical Processes. *Chem. Mater.* **2000**, *12*, 1591–1596.